China Geology 7 (2024) 277–290

China Geology

Journal homepage: http://chinageology.cgs.cn
https://www.sciencedirect.com/journal/china-geology

Extensive identification of landslide boundaries using remote sensing images and deep learning method

Chang-dong Li[a, b,*], Peng-fei Feng[c], Xi-hui Jiang[a], Shuang Zhang[d], Jie Meng[a], Bing-chen Li[a]

[a] *Faculty of Engineering, China University of Geoscience, Wuhan* 430074, *China*
[b] *Badong National Observation and Research Station of Geohazards, China University of Geosciences, Wuhan* 430074, *China*
[c] *School of Mechanical Engineering and Electronic Information, China University of Geosciences, Wuhan* 430074, *China*
[d] *College of Geology Engineering and Geomatics, Chang'an University, Xi'an* 710054, *China*

ARTICLE INFO

Article history:
Received 12 December 2023
Received in revised form 3 April 2024
Accepted 8 April 2024
Available online 23 April 2024

Keywords:
Geohazard
Landslide boundary detection
Remote sensing image
Deep learning model
Steep slope
Large annual rainfall
Human settlements
Infrastructure
Agricultural land
Eastern Tibetan Plateau
Geological hazards survey engineering

ABSTRACT

The frequent occurrence of extreme weather events has rendered numerous landslides to a global natural disaster issue. It is crucial to rapidly and accurately determine the boundaries of landslides for geohazards evaluation and emergency response. Therefore, the Skip Connection DeepLab neural network (SCDnn), a deep learning model based on 770 optical remote sensing images of landslide, is proposed to improve the accuracy of landslide boundary detection. The SCDnn model is optimized for the over-segmentation issue which occurs in conventional deep learning models when there is a significant degree of similarity between topographical geomorphic features. SCDnn exhibits notable improvements in landslide feature extraction and semantic segmentation by combining an enhanced Atrous Spatial Pyramid Convolutional Block (ASPC) with a coding structure that reduces model complexity. The experimental results demonstrate that SCDnn can identify landslide boundaries in 119 images with MIoU values between 0.8 and 0.9; while 52 images with MIoU values exceeding 0.9, which exceeds the identification accuracy of existing techniques. This work can offer a novel technique for the automatic extensive identification of landslide boundaries in remote sensing images in addition to establishing the groundwork for future investigations and applications in related domains.

1. Introduction

Severe meteorological events, especially continuous regional heavy rains, often lead to the deterioration of rock and soil structures (Dahal R 2008; Zhang TL et al., 2020; Meng J et al., 2023), thereby easily triggering landslides and resulting in significant loss of lives and property (Li C et al., 2021; Cao WG et al., 2023). After the occurrence of a landslide, the morphological and color distinctions between the landslip body and the surrounding landforms provide the possibility of accurately identifying the boundaries of the landslide. However, this task still confronts significant challenges in practice. Conventional methods for detecting landslides depend on field surveys and manual interpretation, which are labor- and time-intensive procedures that are nearly hard to carry out following a large-scale landslide event (Wei FQ et al., 2010; Lü ZY et al., 2018; Dai C et al., 2021; Liu P et al., 2021). Thus, the solution to this issue currently lies in the automatic identification of landslide boundaries employing remotely sensed pictures (Liu Y et al., 2016; Li Y et al., 2023).

A key approach to mitigating the impact of these natural disasters is the automatic identification of landslide boundaries from remotely sensed imagery (Bragagnolo L et al., 2021; Mohan A et al., 2021). It is possible to promptly gather extensive surface information with remote sensing technology, which is vital for prompting response and post-disaster assessment (Qi T et al., 2021; Zhang X et al., 2023; Feng PF et al., 2024). Unprecedented potential for landslide identification has emerged as the rapid advancements in remote sensing technology, which enables us to obtain images with higher resolution and faster update frequency (Mondini AC et al., 2011; Zhong C et al., 2012; Sun Q et al., 2015;

First author: *E-mail address*: lichangdong@cug.edu.cn (Chang-dong Li).

* Corresponding author: *E-mail address*: lichangdong@cug.edu.cn (Chang-dong Li).

Literary editor: Li-qiong Jia
doi:10.31035/cg2023148
2096-5192/© 2024 China Geology Editorial Office.

Czikhardt R et al., 2017; Zhao C et al., 2018; Solari L et al., 2020). This approach possesses significant potential, particularly in remote or hazardous regions where on-site surveys are impractical.

Remote sensing image analysis has been revolutionized by breakthroughs in deep learning, particularly with regard to convolutional neural network (CNN) for image recognition and classification tasks (Simonyan K et al., 2014; LeCun Y et al., 2015; Krizhevsky A et al., 2017; Zhu XX et al., 2017; Zhou PC et al., 2021). Contrasting to conventional machine learning techniques, these models are capable of understanding the deep features of an image and producing more accurate results (Ghorbanzadeh O et al., 2019; Wang H et al., 2021). However, even if state-of-the-art models, such as Segnet, Mobilenetv2, DeepLab v3^{+} and others work effectively on a variety of complicated image processing tasks, they still encounter several challenges when deployed particularly for landslide boundary detection (Badrinarayanan V et al., 2015; Ding A et al., 2016; Chen LC et al., 2018; Sandler M et al., 2018). The primary issue is that these models tend to over-segment when presented with scenarios where the topography and geomorphological characteristics closely resemble the surrounding area. In practical applications, this over-segmentation results in substantially lower accuracy because it not only captures erroneous landslide boundaries but also misclassifies non-landslide areas.

These limitations stem mostly from the fact that traditional CNN models are designed without a thorough comprehension of the inherent variability of complicated terrain features (Xu C et al., 2020). Typically, they fall short when it comes to extracting high-level semantic information and integrating global contextual information, particularly in high-complex and large-scale datasets, such as remote sensing images (Li Y et al., 2021; Long Y et al., 2021). It is required to develop new network architectures that can handle multi-scale information and intricate textures in images, in addition to being more finely tuned in feature extraction, to overcome these constraints. Additionally, models are supposed to adjust to deficiencies in the datasets to avoid overfitting and maintain the capacity for generalizing to unknown landslide images.

The novel deep learning model-Skip Connection DeepLab neural network (SCDnn), which is built on the enhanced DeepLab v3^{+} framework, is proposed here to overcome the aforementioned problems. Through structural optimisation, the SCDnn model greatly increases the detection accuracy of landslide boundaries. The pooling channel in Atrous Spatial Pyramid Pooling Block (ASPP) is eliminated through SCDnn by introducing the Atrous Spatial Pyramid Convolutional Block (ASPC), which lowers the number of parameters and computational complexity. Furthermore, SCDnn leverages parallel structures, such as Maximum Pooling Downsampling Block and Mixed Residual, to lessen the depth of the model and reliance on a substantial amount of training data while also improving the generalization ability of the model.

2. Study area and applied data

The study area is located in the northwest of Guizhou province, China, spanning from latitude 26°21' to 27°46' North and longitude 103°36' to 106°43' East (Fig. 1a). Covering the entire Bijie City, with a total area of 26853 km². This region lies within the transition zone from the Tibetan Plateau to the eastern hilly area with the elevation ranging from 457 m to 2900 m above sea level (a.s.l.). The geological setting of this area is relatively fragile and instability, which is characterized by incompetent strata, intensively developed foldings and faultings, steep hillsides and substantial annual rainfall (averaging between 849 mm and 1399 mm). These factors collectively make it one of the most landslide-prone areas in China. The primary types of landslides in Bijie City include rock falls and rock slides, with occasional debris slides. Each year, this region experiences a significant number of new landslides, some of which pose severe threats to human settlements, infrastructure, and agricultural lands.

To validate the efficacy of the proposed approach for

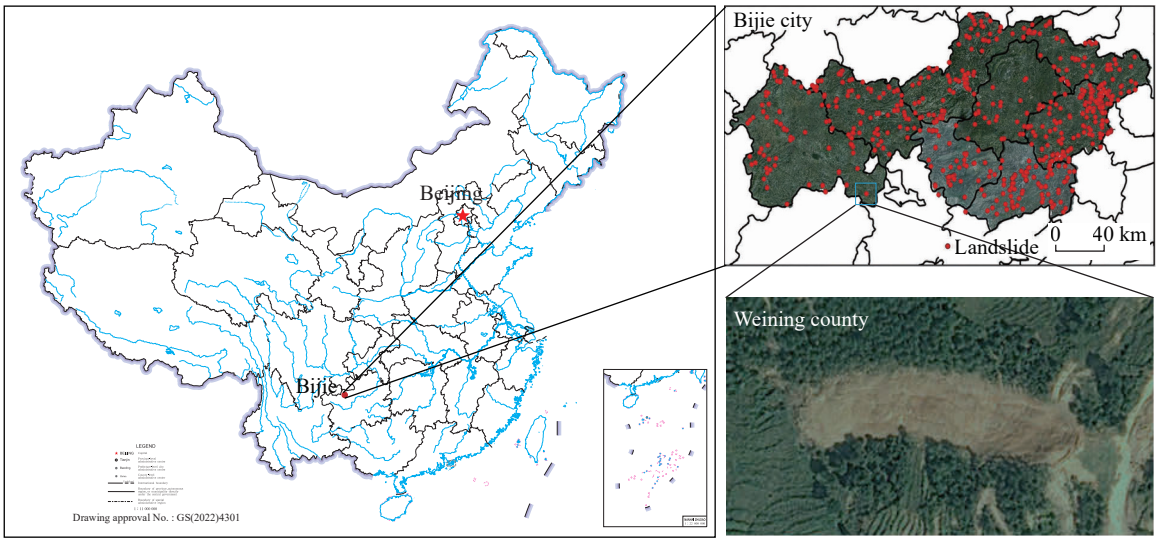

Fig. 1. Study area map of the Three Gorges Reservoir, with the landslide images. The sourced from the research of Ji S et al. (2020).

accurate landslide location and boundary detection, this study focuses on landslides thoroughly investigated in Bijie City, Guizhou Province. Landslide data were collected and processed within this study area. The dataset, constructed by Ji S et al. (2020), consists of 770 samples of Bijie City landslides, identified using TripleSat satellite images taken from May to August 2018 (Fig. 2).

3. Methodology

3.1. Skip Connection DeepLab neural network

Current research on segmenting landslide morphological boundaries from remote sensing images and designing deep learning models for this purpose is relatively limited. However, several segmentation models such as SegNet, U-Net, and the DeepLab series have been developed in the fields of semantic and image segmentation, capable of precisely segmenting each part of an image (Ronneberger O et al., 2015). Therefore, this study constructs a model based on the DeepLab v3+ framework, suitable for the semantic segmentation of landslide images. Fig. 3 shows the architecture diagram of this new model, named the Skip Connection DeepLab neural network (SCDnn), which includes the coding module, Atrous Spatial Pyramid Convolutional Block (ASPC) and the decoding module.

The coding module is designed for extracting landslide features and downsampling, capturing the semantic information of the input image and transforming it into a richer feature representation. This module contains multiple convolutional and pooling layers to capture details of landslide images across different scales, forms, and colors, preparing for subsequent semantic segmentation tasks. The ASPC, an improvement over the ASPP (Chen LC et al., 2017), aims to enhance semantic segmentation performance by extracting features of landslide images at various receptive field scales. The ASPC module uses convolution operations with different atrous rates to capture semantic information at various scales, from local to global.

The role of the decoding module is to upsample and recover the details of the segmentation results, generating a high-resolution semantic segmentation map. Through upsampling, the decoding module restores the low-resolution feature maps from the coding module to the original image size for pixel-level semantic classification. It also combines multi-scale feature maps from the ASPC and coding modules, improving the accuracy of the segmentation results and enhancing the edge information, thereby better capturing the details and contours of the landslide body. Ultimately, the decoding module uses a convolution operation to create a mask map for the semantic segmentation of the landslide, assigning each pixel in the image to a corresponding semantic category.

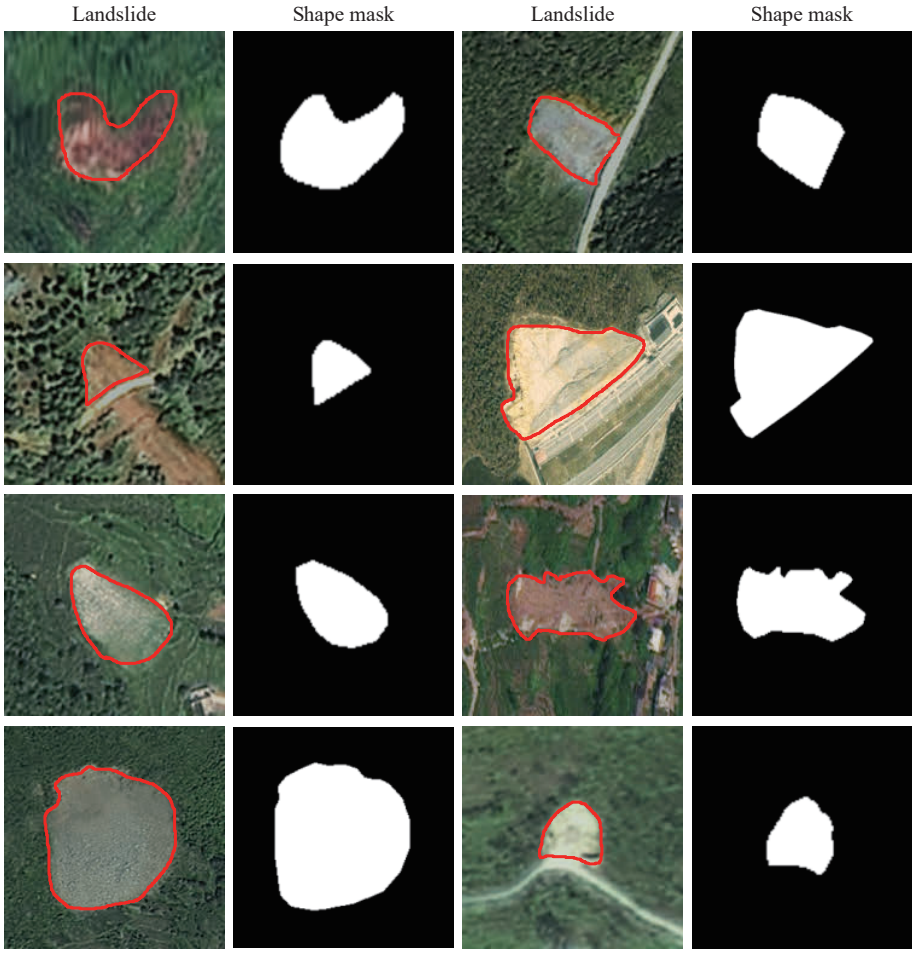

Fig. 2. Bijie landslide image and landslide shape mask dataset, with the landslide images. The sourced from the research of Ji S et al. (2020).

3.1.1. Mixed Residual and Maximum Pooling Downsampling Block

In the SCDnn system, Mixed Residual and Maximum Pooling Downsampling Block (MRmaxpooling Downsampling Block) is the first group of coding modules that performs a crucial role in the model. This module encompasses two branching structures: One branch is a feature extraction branch consisting of convolution, normalization and activation functions induced after maxpooling, and the other is a residual branch induced after maxpooling (Fig. 4). An additive connecting layer for element-wise summing eventually connects both branches. This model could be represented as (Equs. 1, 2):

$$F_1 = \mathrm{BN}(\mathrm{Conv3*3}(\mathrm{ReLU}(\mathrm{BN}(\mathrm{Conv3*3}(x))))) \tag{1}$$

$$F_{\mathrm{out}} = F_1 + x \tag{2}$$

where $\mathrm{Conv3*3}$ denotes a convolution operation with a convolutional kernel size of 3*3 (Equ. 3):

$$f(x) = \sum_{u=1}^{\mathrm{U}} \sum_{v=1}^{\mathrm{V}} w_{uv} x_{i+u-1, j+v-1} \tag{3}$$

BN indicates batch normalization (Equ. 4):

$$f(x) = \gamma \left(\frac{x - \mu(x)}{\sigma(x)} \right) \tag{4}$$

$ReLU$ is the activation function of the neuron, making non-linear transformation for input data (Equ. 5):

$$f(x) = \begin{cases} x, & if \quad x > 0 \\ 0, & if \quad x \leqslant 0 \end{cases} = \max(0, x) \tag{5}$$

In the aforementioned formulae, x is feature input, i and j denote the coordinate position of the feature input, U and V are the height and width of the convolutional kernel matrix, u and v show the changing coordinates, μ and σ represent mean value and variance respectively, γ means non-linear

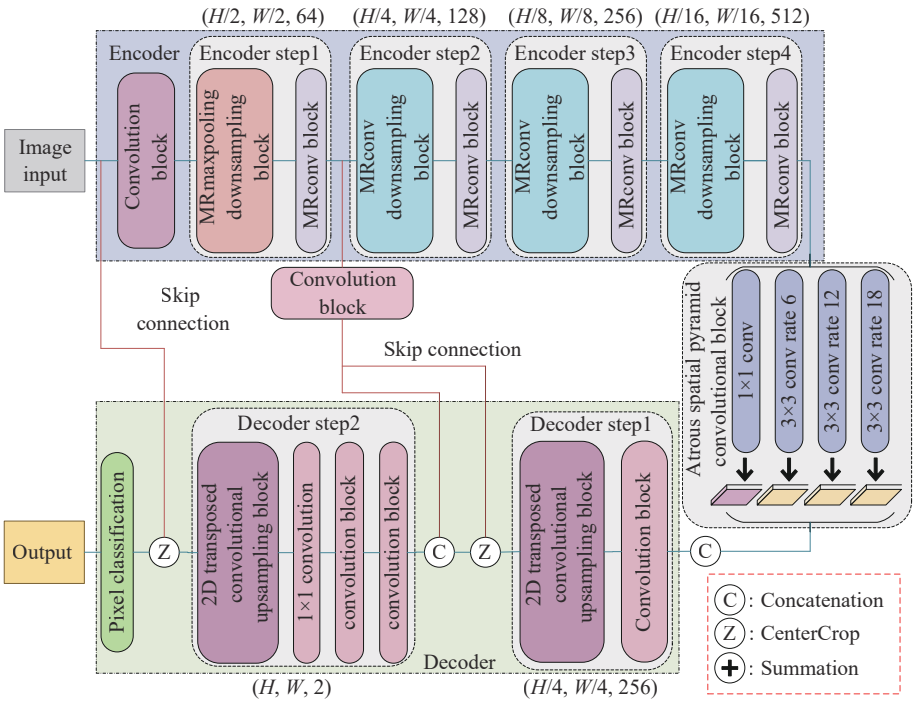

Fig. 3. Architecture of Skip Connection DeepLab neural network.

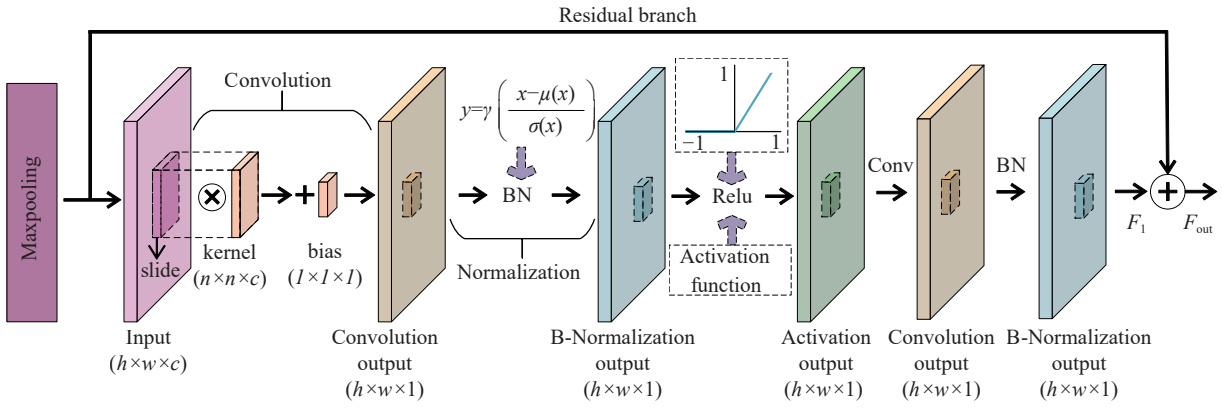

Fig. 4. Mixed residual and maximum pooling downsampling block (legends are same as Fig. 3).

transformation, F_1 indicates the output of the feature extraction branch.

In MRmaxpooling Downsampling Block, the initial stage is to reduce the width and height of the landslide feature maps utilizing the maxpooling layer, i.e., to perform a downsampling operation. Its primary goal is to make the landslide image feature matrix conformed to the dimension of display area and generate the corresponding feature matrix. In addition, maxpooling can acquire local information and better preserve the features on texture. Furthermore, the residual branch learns residual to address deep neural network representation bottleneck and gradient vanishing issues. The major function of the feature extraction branch is feature extraction.

3.1.2. Mixed Residual and Convolutional Downsampling Block

Mixed Residual and Convolutional Downsampling Block (MRconv Downsampling Block) is another significant module in the SCDnn system, applied in groups 2, 3 and 4 coding modules. These two methods, MRmaxpooling Downsampling Block and MRconv Downsampling Block, share the same feature extraction and downsampling functions as well as two branching routes. The distinction is that whilst the convolutional layer with a step size of 2 downsamples MRconv, the downsampling of MRmaxpooling is done by the maxpooling layer. Meanwhile, the maxpooling layer performs the downsampling for MRmaxpooling Downsampling Block prior to entering the branch, whereas the downsampling for MRconv Downsampling Block is carried out independently by each of the two branches after entering the branch. Analogous to MRmaxpooling Downsampling Block, the additive connnecting layer adds elements-by-elements to finally connect both branches (Fig. 5a). The following is the representation of this module (Equs. 6–8).

$$F_1 = \mathrm{BN}(\mathrm{Conv3*3}(\mathrm{ReLU}(\mathrm{BN}(\mathrm{Conv3*3}(x))))) \tag{6}$$

$$F_2 = \mathrm{BN}(\mathrm{Conv1*1}(x)) \tag{7}$$

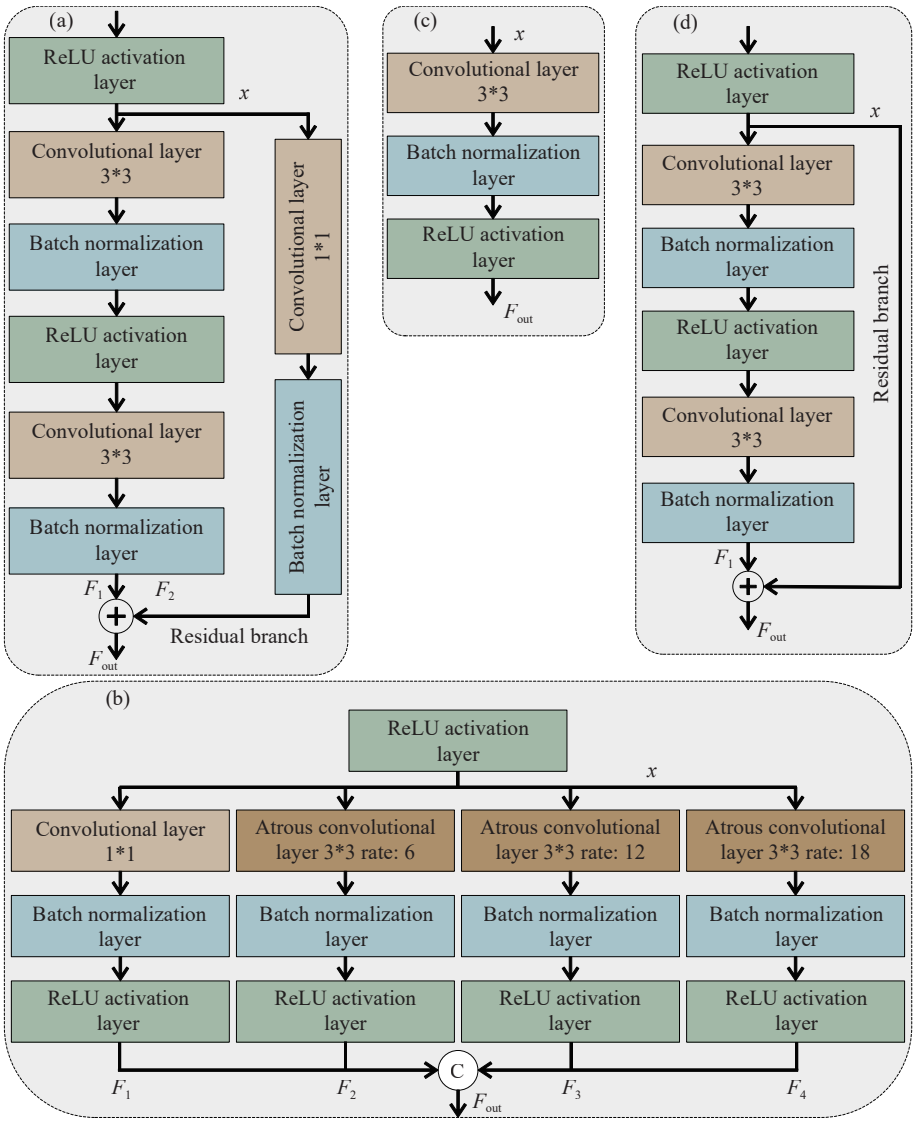

Fig. 5. Other component blocks of SCDnn: a–Mixed residual and convolutional downsampling block; b–Atrous spatial pyramid convolutional block; c–Convolution block; d–Mixed residual and convolutional block (legends are same as Fig. 3).

$$F_{out} = F_1 + F_2 \tag{8}$$

In these equations, x represents the landslide feature input matrix, F_1 and F_2 are the outputs of both branches respectively, Conv1*1 and Conv3*3 denote the convolution operation with the convolutional kernel size of 1*1 and 3*3 respectively. Eventually, the outputs of both branches are summed by an additional operation to obtain the final output of the hybrid downsampling module. With the aid of this structure, the network is better able to learn how to lower the resolution while maintaining an efficient representation of the features.

3.1.3. Atrous Spatial Pyramid Convolutional Block

In the SCDnn system, Atrous Spatial Pyramid Convolutional Block (ASPC) is the most core module. Four branching structures, with each involving a convolutional layer, a normalization layer, and an activation function layer, constitute this module (Fig. 5b). The main difference lies on that a general 1*1 convolutional structure is employed in the convolutional layer of the first branch structure, while the other branch structures utilize a unique atrous convolutional structure with their sampling rates being 6, 12 and 18. The module can be expressed as follows (Equs. 9–13):

$$F_1 = \mathrm{ReLU}(\mathrm{BN}(\mathrm{Conv1} * 1(x))) \tag{9}$$

$$F_2 = \mathrm{ReLU}\left(\mathrm{BN}\left(\mathrm{Conv3} * 3^{rate6}(x)\right)\right) \tag{10}$$

$$F_3 = \mathrm{ReLU}\left(\mathrm{BN}\left(\mathrm{Conv3} * 3^{rate12}(x)\right)\right) \tag{11}$$

$$F_4 = \mathrm{ReLU}\left(\mathrm{BN}\left(\mathrm{Conv3} * 3^{rate18}(x)\right)\right) \tag{12}$$

$$F_{out} = \begin{bmatrix} F_1 & F_2 & F_3 & F_4 \end{bmatrix} \tag{13}$$

Different branches of the ASPC Block process the input feature maps at different scales to capture information at varying sampling rates. This allows the model to identify objects or details at small scales while also process contextual information at large scales. The performance of semantic segmentation is enhanced by ASPC Block through convolution procedures, which expand the receptive field of each pixel and allow the network to comprehend information from a larger area. The atrous convolution in ASPC Block, also referred to as dilated convolution, achieves an increase in the effective receptive field of the convolution kernel by introducing atrous between the convolution kernels with no further parameters added. Overall, ASPC Block increases the performance of image semantic segmentation tasks by efficiently capturing contextual information at different scales using atrous pooling and convolutional kernels with multi-scale sampling rates.

3.1.4. 2D transposed Convolutional Upsampling Block

A crucial module in SCDnn system, 2D Transposed Convolutional Upsampling Block, serves to upsample and restore feature map resolution. In actuality, 2D transposed Convolution is a type of the inverse convolution procedure, occasionally referred to as deconvolution. It extends the feature map by inserting zeros and then utilizes convolution kernels to fill these zeros, thus enabling up-sampling. As a result, it is able to upsample the low-resolution feature maps to a higher resolution, further recovering vital detail information of the objects in the landslide feature maps. The following is a summary of the 2D transposed convolution procedure.

Assume that the sparse matrix C of the convolutional kernel is represented as follows (Equ. 14):

$$C = \begin{bmatrix} w_{11} & w_{12} & 0 & w_{21} & w_{22} & 0 & 0 & 0 & 0 \\ 0 & w_{11} & w_{12} & 0 & w_{21} & w_{22} & 0 & 0 & 0 \\ 0 & 0 & 0 & w_{11} & w_{12} & 0 & w_{21} & w_{22} & 0 \\ 0 & 0 & 0 & 0 & w_{11} & w_{12} & 0 & w_{21} & w_{22} \end{bmatrix} \tag{14}$$

Let the input to the transposed convolution be (Equ. 15):

$$X = \begin{bmatrix} x_{11} & x_{12} \\ x_{21} & x_{22} \end{bmatrix} \tag{15}$$

The corresponding vector of this input is (Equ. 16):

$$x' = \begin{bmatrix} x_{11} & x_{12} & x_{21} & x_{22} \end{bmatrix}^T \tag{16}$$

So the outcome of the 2D transposed convolution is (Equ. 17):

$$Y = C^T x' = \begin{bmatrix} w_{11}x_{11} & w_{12}x_{11} + w_{11}x_{12} & w_{12}x_{12} \\ w_{21}x_{11} + w_{11}x_{21} & w_{22}x_{11} + w_{21}x_{12} + w_{12}x_{21} + w_{11}x_{22} & w_{22}x_{12} + w_{12}x_{22} \\ w_{21}x_{21} & w_{22}x_{21} + w_{21}x_{22} & w_{22}x_{22} \end{bmatrix} \tag{17}$$

The decoding stage of the SCDnn model deploys two 2D Transposed Convolutional Upsampling Blocks, each of which progressively restores the detailed information of the object by increasing the resolution of feature map at a four-fold magnification frequency. This multi-scale upsampling operation improves the performance of the model in segmenting the landslide body from the background. In the meantime, the 2D transposed convolution functions to enlarge the feature map, matching its to the size feature map during the downsampling procedure through skip connection. This facilitates the information from the top and bottom feature maps to be organically integrated resulting in superior segmentation outcomes.

3.1.5. Other Blocks

In the SCDnn system, Convolution Block, Mixed Residual and Convolutional Block (MRconv Block), Skip Connection, and Pixel Classification are all the general module of neural network (Figs. 5c, d). A convolutional layer, a batch normalization layer, and a relu activation layer

compose a convolution block. In each Convolution Block, the convolution layer takes the output of the previous layer as its own input, and generates a new feature map by performing feature extraction operations in local regions. The primary role of the batch normalization layer is to normalize each batch of input data to enhance the generalization ability of the model and speed up the training process. On the other side, nonlinear features are introduced by the ReLU activation function, allowing the network to learn more intricate patterns. The section can be demonstrated as follows (Equ. 18):

$$F_{out} = \mathrm{ReLU}(\mathrm{BN}(\mathrm{Conv3*3}(x))) \tag{18}$$

The MRconv Block and the MRconv Downsampling Block are structurally and functionally identical; the only distinction remains that the MRconv Block lacks a normalization layer and a convolutional layer in the residual branch and features a convolutional layer with a step size of 1 without downsampling function. The key role it plays in deep neural network training is to resolve the gradient vanishing and gradient explosion issues, enabling training of extremely deep neural networks. Additionally, it could achieve higher classification accuracy and generalization ability since it is more adept at capturing the abstract features in the image. A representation of this module would be (Equ. 19):

$$F_{out} = \mathrm{BN}(\mathrm{Conv3*3}(\mathrm{ReLU}(\mathrm{BN}(\mathrm{Conv3*3}(x))))) + x \tag{19}$$

SCDnn utilizes Skip Connection to fuse information from both lower and higher-level features, preserving details to enhance segmentation performance and augment the model's expressive power. The final layer of the model, Pixel Classification, is responsible for categorizing each pixel in an image into a predefined semantic category. It allows the model to segment the image into distinct objects and regions, providing semantic labels for each pixel. Prior to Pixel Classification, a softmax layer is introduced to normalize the model's output, converting each pixel's output into distributions that represent the probability of each category. This means the model can predict the probability of each pixel in a given image belonging to each category. Specifically, the softmax layer maps each component of the output vector of each pixel to a probability value that sums to 1, offering more reliable and comprehensible predictions in classification tasks and helping to interpret the model's output as a probability distribution of categories.

Through the integration of these Blocks, this research successfully accomplished the encoding and decoding of landslide images, translating the high-level feature representation of the image into probability distributions of classification predictions for individual pixel points. This design allows the model to accomplish accurate segmentation and boundary detection of landslide images on the basis of processing feature extraction and fusion.

3.2. Training and optimization of the network model

SCDnn is a kind of deep neural network with a convolutional structure. The convolution layer and pooling sub-layer of the hidden layer are the core modules that realize the feature extraction function of a SCDnn. The network model adopts the gradient descent method to minimize its loss function, adjusts the weight parameters layer by layer, and achieves improved network accuracy through frequent iterative training.

Adaptive moment estimation (Adam) is a stochastic optimization method that requires only one step (Kingma DP et al., 2014). The method calculates the individual adaptive learning rates of different parameters from the estimations of the first moment and the second moment of the gradient. The design of this method combines the advantages of two popular methods: AdaGrad (Duchi J et al., 2011), which works well with sparse gradients, and RMSProp (Tieleman T et al., 2012), which works well in online and nonstationary settings. Some of Adam's advantages are that the magnitudes of its parameter updates are invariant to gradient rescaling, its step sizes are approximately bounded by the step size hyperparameter, it does not require a stationary objective, it works with sparse gradients, and it naturally performs a form of step size annealing. The pseudocode flow of the algorithm is as follows.

Require: α **:** Step size

Require: $\beta_1, \beta_2 \in [0,1)$: Exponential decay rates for the moment estimates

Require: $f(\theta)$: Stochastic objective function with parameters θ

Require: θ_0 : Initial parameter vector

$m_0 \leftarrow 0$ (Initialize 1st moment vector)

$v_0 \leftarrow 0$ (Initialize 2nd moment vector)

$t \leftarrow 0$ (Initialize time step)

While θ_t not converged **do**

$t \leftarrow t+1$

$g_t \leftarrow \nabla_\theta f_t(\theta_{t-1})$ (Get gradients w.r.t. stochastic objective at time step t)

$m_t \leftarrow \beta_1 \cdot m_{t-1} + (1-\beta_1) \cdot g_t$ (Update biased first moment estimate)

$v_t \leftarrow \beta_2 \cdot v_{t-1} + (1-\beta_2) \cdot g_t^2$ (Update biased second raw moment estimate)

$\hat{m}_t \leftarrow m_t / (1-\beta_1^t)$ (Compute bias-corrected first moment estimate)

$\hat{v}_t \leftarrow v_t / (1-\beta_2^t)$ (Compute bias-corrected second raw moment estimate)

$\theta_t \leftarrow \theta_{t-1} - \alpha \cdot \hat{m}_t / \left(\sqrt{\hat{v}_t} + \varepsilon\right)$ (Update parameters)

end while

return θ_t (Resulting parameters)

g_t^2 indicates the element-wise square $g_t \cdot g_t$. Good default settings for the tested machine learning problems are $\alpha = 0.001$, $\beta_1 = 0.9$, $\beta_2 = 0.999$ and $\varepsilon = 10^{-8}$. All operations on vectors are element-wise. With β_1^t and β_2^t, we denote β_1 and β_2 to the power t.

4. Experiment analysis

4.1. Experimental environment setting

Seventy percent of the landslide dataset, consisting of landslide photographs and landslide form mask images, is classified as a test set in these studies, whereas the remaining thirty percent is classed as a training set. Matlab R2023a is implemented to accomplish the suggested approach on intel CORE i7-10750H CPU and NVIDIA 1650 Ti GPU computer equipped with 16 GB of RAM. Models, such as Simple Semantic Segmentation Network (SSSN), Segnet (Badrinarayanan V et al., 2015), DeepLab v3$^+$ network based on ResNet50 (He K et al., 2016; Chen LC et al., 2018), and DeepLab v3$^+$ network based on Mobilenetv2 (Chen LC et al., 2018; Sandler M et al., 2018) that are deployed for comparative experiments will all exclude pre-trained parameters, i.e., the initial unpretrained model will be applied. Every model employs the identical training parameters while undertaking training.

The experimental findings are compared with five evaluation criteria, Pixel Accuracy (PA), Mean Pixel Accuracy (MPA), Intersection over Union (IoU), Mean Intersection over Union (MIoU) and Frequency Weighted Intersection over Union (FWIoU), to achieve a comprehensive and precise assessment of all the network models. PA refers to "the proportion of the number of pixels with the correct prediction classification to the total number of pixels". The calculation formula is (Equ. 20):

$$PA = \frac{\sum_{i=0}^{k} p_{ii}}{\sum_{i=0}^{k}\sum_{j=0}^{k} p_{ij}} \tag{20}$$

where k denotes the number of classifications of pixels, which is landslide and background in this research. Consequently, the number of classification is 2; p_{ii} means that the pixel point of category i of the pixel is correctly predicted to be i; p_{ij} indicates that the error prediction of pixels of category i is j; p_{ji} is a pixel of class j incorrectly predicted as i.

MPA stands for mean percentage of correctly classified pixels in each class, which is computed individually and then averaged over time. Its formula is expressed as follows (Equ. 21):

$$MPA = \frac{1}{k+1}\sum_{i=0}^{k} \frac{p_{ii}}{\sum_{j=0}^{k} p_{ij}} \tag{21}$$

IoU denotes the ratio of the intersection and concatenation of the predicted results and true values for a category, i.e., it calculates the intersection and concatenation ratio between the predicted and true masks (Equ. 22).

$$IoU = \frac{\sum_{i=0}^{k} p_{ii}}{\sum_{i=0}^{k}\left(\sum_{j=0}^{k} p_{ij} + \sum_{j=0}^{k} p_{ji} - p_{ii}\right)} \tag{22}$$

MIoU indicates the ratio of the intersection and concatenation of the true value and the prediction results of each class. Then the ratios of each category are summed, and the average of the ratios is calculated. The formula for calculation is (Equ. 23):

$$MIoU = \frac{1}{k+1}\sum_{i=0}^{k} \frac{p_{ii}}{\sum_{j=0}^{k} p_{ij} + \sum_{j=0}^{k} p_{ji} - p_{ii}} \tag{23}$$

As an enhancement of MIoU, FWIoU sets weights to each class according to how frequently it occurs. The following is the calculating formula (Equ. 24):

$$FWIoU = \frac{1}{\sum_{i=0}^{k}\sum_{j=0}^{k} p_{ij}}\sum_{i=0}^{k} \frac{\sum_{j=0}^{k} p_{ij} p_{ii}}{\sum_{j=0}^{k} p_{ij} + \sum_{j=0}^{k} p_{ji} - p_{ii}} \tag{24}$$

MIoU is the most commonly utilized metric among all the evaluation criteria described above because of its representativeness and simplicity.

4.2. Results analysis of different network model architectures

The proposed SCDnn is trained and forecasted together with the comparison models SSSN, Segnet, DeepLab v3$^+$ network based on ResNet50, and DeepLab v3$^+$ network based on Mobilenetv2, where the prediction results of SCDnn are displayed applying a normalized confusion matrix (Table 1). Table 2 illustrates the landslide segmentation results of different network architecture models for the entire landslide dataset.

In this work, 231 landslide images were segmented and identified using the proposed SCDnn model in practical tests. Nevertheless, the model makes some errors in the identification of landslide pixel points, it misidentifies 1.04% of non-landslide picture pixel points as landslide pixel points and mistakenly labels 25.89% of landslide pixel points as non-landslide pixel points, as illustrated in Table 1. These data demonstrate that the SCDnn model could identify landslides segmentation with considerable accuracy, but misidentification still occurs occasionally. Even so, the SCDnn model still outperforms them in terms of segmentation performance of landslide images over the entire dataset, with a high MIoU value of 82.14%, and higher PA, MPA, and FWIoU metrics than other models (Table 2). In addition, through the comprehensive analysis of the landslide shape

Table 1. SCDnn test result normalized confusion matrix.

SCDnn		Predicted label	
		Landslide	Background
Actual label	Landslide	0.7411	0.2589
	Background	0.0104	0.9896

Table 2. Landslide segmentation results of different network architecture models of the entire landslide dataset.

Model	PA	MPA	MIoU	FWIoU
SSSN	88.75%	53.08%	47.64%	79.46%
Segnet	82.60%	70.98%	54.00%	75.26%
ResNet50	94.13%	86.11%	76.41%	89.72%
Mobilenetv2	94.71%	84.38%	77.22%	90.42%
SCDnn	96.16%	86.54%	82.14%	92.74%

masks generated from the segmented landslide images by each model, it could be discovered from Fig. 6 that the SCDnn model is able to segment and identify landslide borders with greater accuracy and clarity in comparison to other network model. This suggests that the model is highly accurate and superior at segmenting numerous images of landslides.

The SSSN network model outperforms the SCDnn model in terms of PA for the Background category in the segmentation results of different network architectural models for a single class of landslide dataset, i.e., the segmentation of landslides and background (Table 3). These outcomes can be attributed to the fact that the SSSN model segmented and identified background and landslide pixels as background across the image (Fig. 7a). As a result, the Background category obtained a high PA value, while the Landslide category had a low value of 7.02%. Meanwhile, ResNet50 splits the pixel points of the Background category in addition to the Landslide category, which elucidates why the SCDnn model performs worse than the ResNet50 model in terms of PA on the Landslide category (Fig. 7b). Accordingly, the segmentation performance of the ResNet50 model is 96.46% for Background category PA, which is less than 98.96% of the SCDnn model(Table 3). This is also a side note that a single measure of PA value is biassed.

The SCDnn model developed in this research surpasses all other network models in terms of the balanced assessment IoU values for individual categories of landslide segmentation. This benefit is exhibited in the fact that, when handling the landslide segmentation task, the SCDnn model is able to segment and identify the shape and boundaries of the actual landslide body with greater accuracy (Fig. 6). It implies that when dealing with regions with geomorphology similar to the landslip body, the model can effectively avoid the over-segmentation issue to some extent. At the same time, the model could identify non-landslide body areas more accurately. The SCDnn model performs relatively high practicability and robustness for landslide body segmentation tasks as a result of these characteristics.

4.3. Optimization of SCDnn model for numerous landslide boundary identification

The SCDnn model exhibits exceptional accuracy performance in the domain of landslide accurate location and boundary identification segmentation, as demonstrated by a comprehensive analysis of the confusion matrix in Table 1 and the prediction results of various deep learning network models in Table 2. In the validation test on 231 images, MIoU values above 0.9 are observed in roughly 22.51% of the landslide segmentation results. Approximately 51.52% of the test dataset consisted of a significant portion of test images with landslide segmentation results achieving MIoU values between 0.8 and 0.9, as displayed in Fig. 8. Nearly three quarters of the test data are accounted for by the sum of the two.

The SCDnn model carried out an excellent task of segmenting landslides from the surrounding mountains, as evidenced by the analysis of the 119 images with MIoU values between 0.8 and 0.9 and the 52 images with MIoU values greater than 0.9. The landslide boundaries obtained are more accurate than those produced by ResNet50 and obilenetv2 with similar performance (Fig. 9 and Table 4). For instance, in Fig. 9a, the segmentation of the SCDnn model identifies the landslide boundary, which is comparatively less

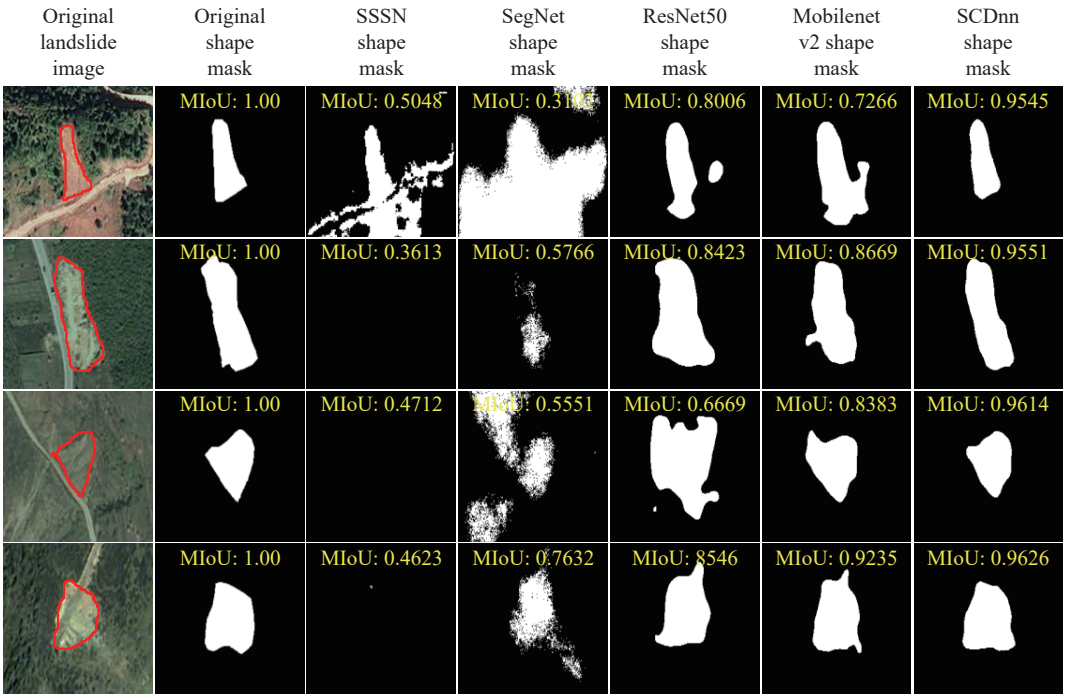

Fig. 6. Segmented images generated by different network architecture models of precise location identification of landslides, with the landslide images. The sourced from the research of Ji S et al. (2020).

over-segmented and considerably more accurate than obtained by the segmentation of ResNet50 and Mobilenetv2. The landslides in area Fig. 9a essentially share the same geomorphology and color as the right side of the mountain, which causes the ResNet50 and MobileNetV2 models to classify parts of the right side of the mountain as landslides as well. Similar situations can be witnessed in Figs. 9b–d, where the model misidentifies the surrounding mountains as landslide bodies in addition to correctly identifying the landslide body itself due to ResNet50 and Mobilenetv2 over-segmenting to the nearby mountains with geomorphology similar to the landslide body. With the SCDnn model, this is comparatively not the case.

One way to elucidate the superior segmentation performance of the SCDnn model over the ResNet50 and Mobilenetv2 models — both of which are built on the deeplab v3$^+$ framework — is that SCDnn enhances the ASPP module in the deeplab v3$^+$ framework to ASPC. With ASPC, only the four distinct scale atrous convolution channels are employed for parallel processing of features with different scales; the parallel pooling channels in the ASPP module with the four convolutional channels are eliminated. This structural design allows the SCDnn model to capture richer information while simultaneously better preserving the spatial information of the image and reducing the amount of parameters. On the other hand, MRmaxpooling Downsampling Block, MRconv Downsampling Block, and MRconv Block in the SCDnn model with a large number of parallel structures can lower the depth and complexity of the model due to the comparatively limited quantity of data in the landslide dataset, hence reducing the demand for training data. The encoding phase of the SCDnn model modelled a network depth that was only about half that of the ResNet50 and Mobilenetv2 models. In addition to preventing overfitting, this enables the SCDnn model to better utilize the information in the data to capture the image's details and edge information. It then enhances the performance of the model and improves segmentation accuracy, better handling complex shapes and textures, noise, and outliers. Ultimately, the SCDnn model is able to locate and identify the majority of landslides with greater accuracy and boundary segmentation of higher quality.

Table 3. Landslide segmentation results of different network architecture models of a single class in the landslide dataset.

Model	Classification	PA	IoU
SSSN	Landslide	7.02%	6.58%
	Background	99.14%	88.69%
Segnet	Landslide	55.99%	26.57%
	Background	85.97%	81.43%
ResNet50	Landslide	75.75%	59.23%
	Background	96.46%	93.59%
Mobilenetv2	Landslide	71.06%	60.19%
	Background	97.71%	94.25%
SCDnn	Landslide	74.11%	68.48%
	Background	98.96%	95.81%

In general, the SCDnn model functions satisfactorily in numerous landslip accurate localization and boundary segmentation identification; however, over-segmentation remains an issue that requires resolution, particularly in areas with comparable geomorphology. This serves as a reminder that, in complicated scene handling, further refinement is still required in the ability to distinguish landslides from their surroundings.

However, not all landslide images yield satisfactory

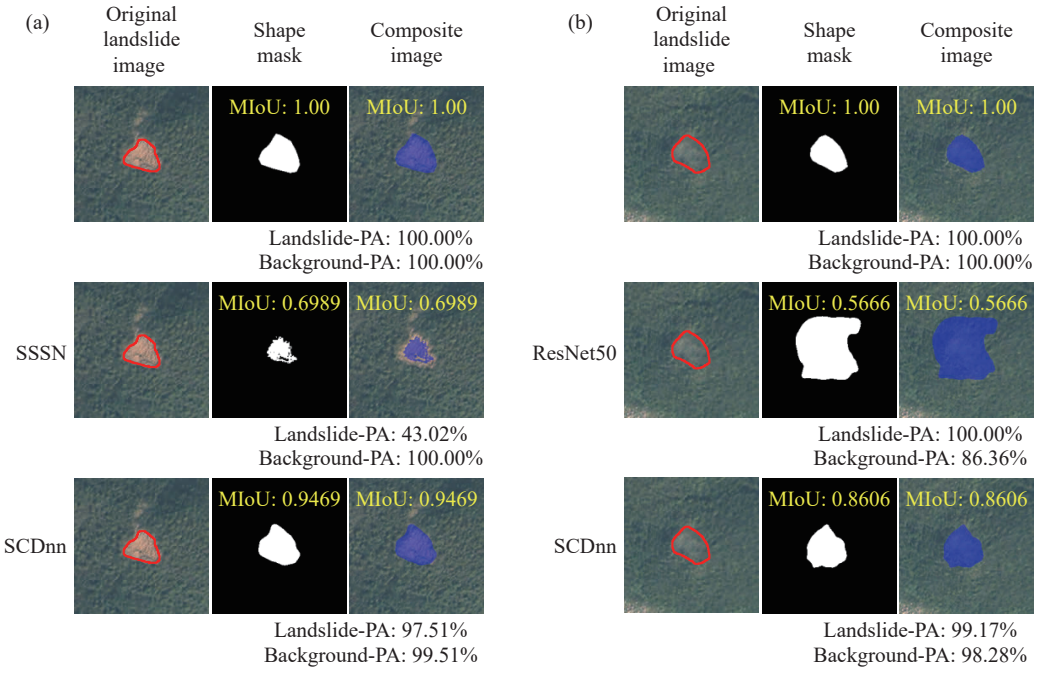

Fig. 7. Segmentation results of different models in individual classes of landslide dataset, with the landslide images sourced from the research of Ji S et al. (2020). a–SSSN and SCDnn models for individual classes of landslide dataset; b–ResNet50 and SCDnn models for individual classes of landslide dataset.

results for landslide border segmentation applying the SCDnn model. There are also 7.79% of test images with landslide segmentation results with MIoU values below 0.7, and even 5 landslide images with MIoU values below 0.6. Upon conducting an in-depth analysis of the five images exhibiting the highest segmentation errors in the SCDnn model, it is evident that these images, possessing MIoU values below 0.6, share a noteworthy characteristic: There are no notable distinctions in the morphology and colour of the landslip and its surrounding areas (Fig. 10). Taking Fig. 10a as an illustration, the SCDnn model classifies the upper and middle portions of the landslip body as background during segmentation since these regions are covered with vegetation, which visually resembles the surrounding area. Nonetheless, the left exposed portion of this landslide body and its right, morphologically distinct portion from its surroundings, have been correctly identified and segmented. Only 17.21% of the landslip body parts were ultimately accurately identified and segmented. As can be witnessed in Figs. 10b–e, the colour of the landslide is practically identical to that of the nearby landforms, and its overall morphology resembles that of the surroundings with morphological boundary differences only in some minor details. The majority of the identified and segmented portions of the landslide are located in the center of the landslide, whereas the SCDnn model could only identify and segment the parts of the landslide that exhibit morphological distinctions in the details. Hence, the SCDnn model still serves some localization purpose even though it fails precisely identify and segment the landslide boundaries in these images.

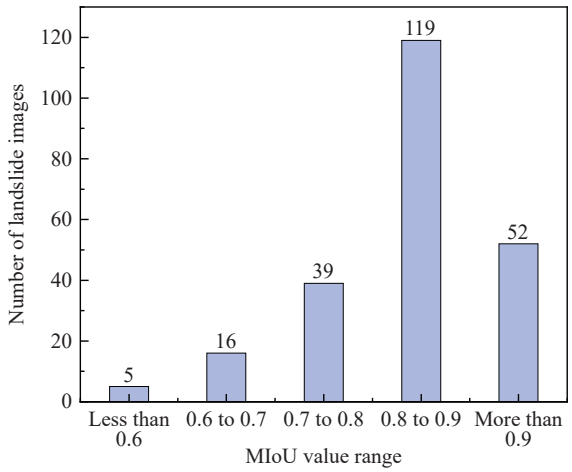

Fig. 8. Statistics of the range of individual image's MIoU values of the segmentation results of the SCDnn model in the landslide dataset.

5. Conclusions

This study developed the SCDnn model, a deep learning

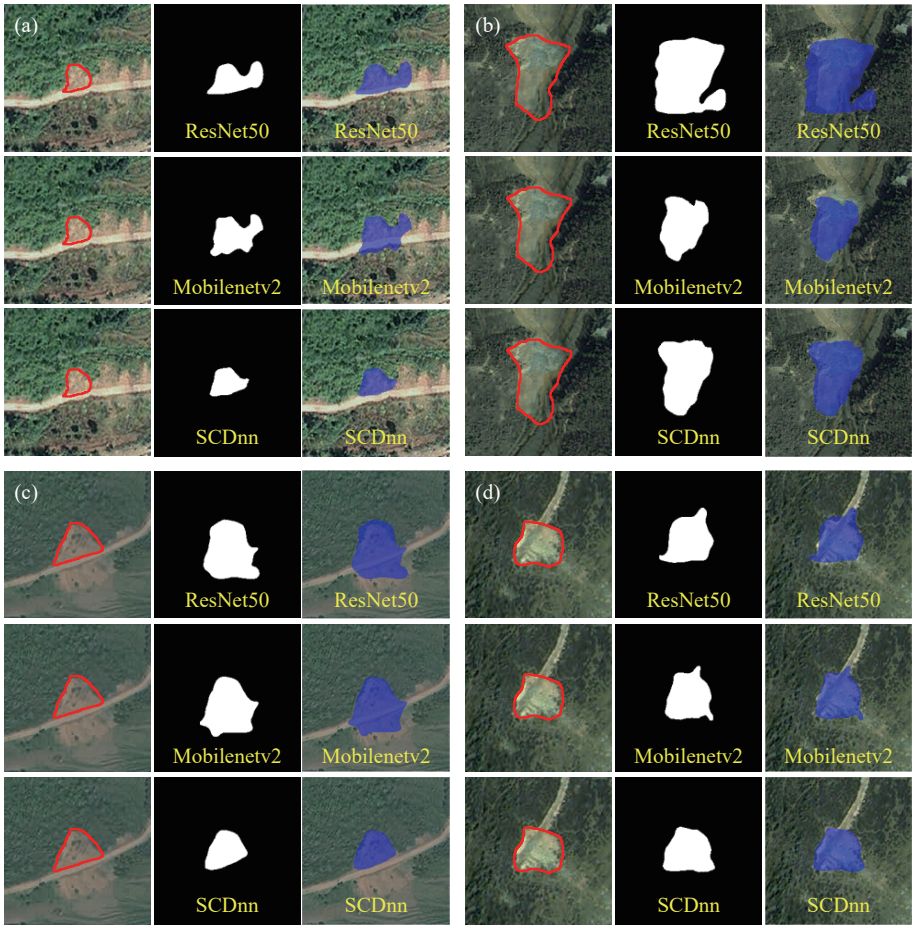

Fig. 9. Some of the remote sensing images and shape masks from SCDnn model with segmentation results' MIoU values between 0.8 and 0.9 and MIoU values larger than 0.9, with the landslide images. The sourced from the research of Ji S et al. (2020).

semantic segmentation tool for segmenting the boundaries of a large number of landslide images. The model is based on the DeepLab v3+ framework and focuses on capturing detailed morphology and boundary characteristics at various scales within landslide images, making it particularly suitable for identifying landslide features. The SCDnn model integrates the innovative ASPC module to replace the traditional ASPP module in the original DeepLab v3+ framework. This integration allows the model to efficiently process multi-scale semantic information with minimal computational overhead, enhancing the fusion of local and global features.

The architecture of the SCDnn model includes strategic parallel structures, such as MRmaxpooling Downsampling Block, MRconv Downsampling Block, and MRconv Block. These elements simplify the depth and complexity of the model, enabling effective data utilization. It thereby reduces the risk of overfitting and ensures the capture of detailed information in complex landslide shapes and textures. The performance of the proposed model demonstrates it effectiveness on a landslide dataset, achieving a Pixel Accuracy (PA) of 96.16% and a Mean Intersection over Union (MIoU) of 82.14%. These results highlight the precision of the SCDnn model in segmenting landslide boundaries and its potential in enhancing landslide disaster monitoring and early warning systems.

CRediT authorship contribution statement

Chang-dong Li, Peng-fei Feng, Shuang Zhang and Jie Meng conceived of the presented idea. Peng-fei Feng, Shuang Zhang, Xi-hui Jiang and Jie Meng carried out the experiment. All authors discussed the results and contributed to the final manuscript.

Declaration of competing interest

The authors declare no conflicts of interest.

Acknowledgment

The research is supported by the National Natural Science Foundation of China (Grant Nos. 42090054, 41931295), the Natural Science Foundation of Hubei Province of China

Table 4. Results for the SCDnn model segmentation show partial MIoU values ranging between 0.8 and 0.9, as well as MIoU values exceeding 0.9 (L-PA represents the PA value of Landslide, B-PA represents the PA value of Background).

	ResNet50			Mobilenetv2			SCDnn		
	L-PA	B-PA	MIoU	L-PA	B-PA	MIoU	L-PA	B-PA	MIoU
Fig. 9(a)	98.52	96.94	0.6861	99.63	95.93	0.6499	100.0	98.99	0.8338
Fig. 9(b)	94.06	92.94	0.7926	62.67	99.18	0.7652	86.03	99.35	0.8996
Fig. 9(c)	99.23	93.70	0.6936	98.12	94.48	0.7108	94.73	99.74	0.9486
Fig. 9(d)	89.35	98.21	0.8546	95.18	99.11	0.9235	94.73	99.74	0.9626

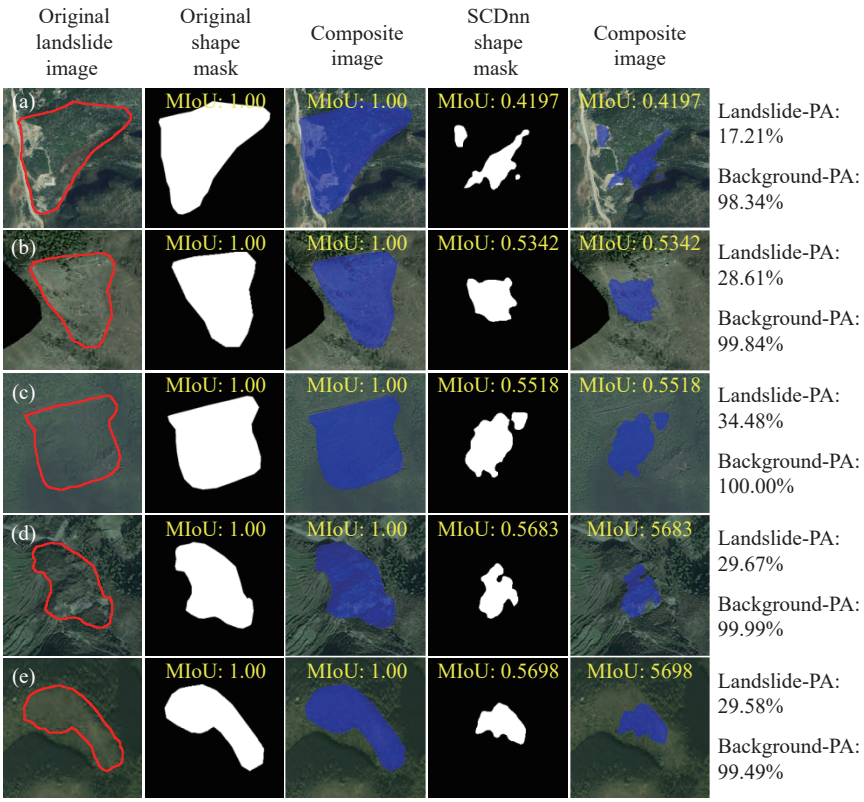

Fig. 10. Some of the remote sensing images and shape masks from SCDnn model with segmentation results' MIoU values less than 0.6, with the landslide images. The sourced from the research of Ji S et al. (2020).

(2022CFA002).

References

Badrinarayanan V, Kendall A, Cipolla R. 2015. Segnet: A deep convolutional encoder-decoder architecture for image segmentation. arXiv. Preprint arXiv: 1511.0051, 2015. doi: 10.48550/arXiv.1511.00561.

Bragagnolo L, Rezende LR, Silva RV, Grzybowski JMV. 2021. Convolutional neural networks applied to semantic segmentation of landslide scars. CATENA, 201, 105189. doi: 10.1016/j.catena.2021.105189.

Cao WG, Fu Y, Dong QY, Wang HG, Ren Y, Li ZY, Du YY. 2023. Landslide susceptibility assessment in Western Henan Province based on a comparison of conventional and ensemble machine learning. China Geology, 6(3), 409–419. doi: 10.31035/cg2023013.

Chen LC, Papandreou G, Kokkinos I, Murphy K, Yuille AL. 2017. Deeplab: Semantic image segmentation with deep convolutional nets, atrous convolution, and fully connected crfs. IEEE transactions on pattern analysis and machine intelligence, 40(4), 834–848. doi: 10.1109/TPAMI.2017.2699184.

Chen LC, Zhu Y, Papandreou G, Schroff F, Adam H. 2018. Encoder-Decoder with Atrous Separable Convolution for Semantic Image Segmentation. In Proceedings of the European conference on computer vision (ECCV), 833–851. doi: 10.48550/arXiv.1802.02611.

Czikhardt R, Papco J, Bakon M, Liscak P, Ondrejka P, Zlocha M. 2017. Ground stability monitoring of undermined and landslide prone areas by means of sentinel-1 multi-temporal InSAR, case study from Slovakia. Geosciences, 7(3), 87. doi: 10.3390/geosciences7030087.

Dahal RK , Hasegawa S , Nonomura A. 2008. Predictive modelling of rainfall-induced landslide hazard in the Lesser Himalaya of Nepal based on weights-of-evidence. Geomorphology, 102 (3–4), 496–510. doi: 10.1016/j.geomorph.2008.05.041.

Dai C, Li WL, Wang D, Lu HY, Xu Q, Jian J. 2021. Active landslide detection based on Sentinel-1 Data and InSAR Technology in Zhouqu County, Gansu Province, Northwest China. Journal of Earth Science, 32(5), 1092–1103. doi: 10.1007/s12583-020-1380-0.

Ding A, Zhang Q, Zhou X, Dai B. 2016. Automatic recognition of landslide based on CNN and texture change detection. 2016 31st Youth Academic Annual Conference of Chinese Association of Automation (YAC), Wuhan, China, 444–448. doi: 10.1109/YAC.2016.7804935.

Duchi J, Hazan E, Singer Y. 2011. Adaptive subgradient methods for online learning and stochastic optimization. Journal of Machine Learning Research, 12(7), 2121–2159. doi: 10.1109/TNN.2011.2146788.

Feng PF, Li CD, Zhang S, Meng J, Long JJ. 2024. Integrating shipborne images with multichannel deep learning for landslide detection. Journal of Earth Science, 35(1), 296–300. doi: 10.1007/s12583-023-1957-5.

Ghorbanzadeh O, Blaschke T, Gholamnia K, Meena SR, Tiede D, Aryal J. 2019. Evaluation of different machine learning methods and deep-learning convolutional neural networks for landslide detection. Remote Sensing, 11(2), 196. doi: 10.3390/rs11020196.

He K, Zhang X, Ren S, Sun J. 2016. Deep residual learning for image recognition. In Proceedings of the IEEE conference on computer vision and pattern recognition, 770–778. doi: 10.1109/CVPR.2016.90.

Ji S, Yu D, Shen C, Li W, Xu Q. 2020. Landslide detection from an open satellite imagery and digital elevation model dataset using attention boosted convolutional neural networks. Landslides, 17(6), 1337–1352. doi: 10.1007/s10346-020-01353-2.

Krizhevsky A, Sutskever I, Hinton GE. 2017. ImageNet classification with deep convolutional neural networks. Communications of the ACM, 60(6), 84–90. doi: 10.1145/3065386.

Kingma DP, Ba J. 2014. Adam: A method for stochastic optimization. arXiv preprint arXiv: 1412.6980. doi: 10.48550/arXiv.1412.6980.

LeCun Y, Bengio Y, Hinton G. 2015. Deep learning. Nature, 521(7553), 436–444. doi: 10.1038/nature14539.

Li C, Criss RE, Fu Z, Long J, Tan Q. 2021. Evolution characteristics and displacement forecasting model of landslides with stair-step sliding surface along the Xiangxi River, three Gorges Reservoir region, China. Engineering Geology, 283, 105961–105975. doi: 10.1016/j.enggeo.2020.105961.

Li Y, Ma J, Zhang Y. 2021. Image retrieval from remote sensing big data: A survey. Information Fusion, 67, 94–115. doi: 10.1016/j.inffus.2020.10.008.

Li Y, Wang P, Feng Q, Ji X, Jin D, Gong J. 2023. Landslide detection based on shipborne images and deep learning models: A case study in the Three Gorges Reservoir Area in China. Landslides, 20(3), 547–558. doi: 10.1007/s10346-022-01997-2.

Liu P, Wei Y, Wang Q, Xie J, Chen Y, Li Z, Zhou H. 2021. A Research on Landslides Automatic Extraction Model Based on the Improved Mask R-CNN. ISPRS International Journal of Geo-Information, 10(3), 168. doi: 10.3390/ijgi1003016.

Liu Y, Wu L. 2016. Geological disaster recognition on optical remote sensing images using deep learning. Procedia Computer Science, 91, 566–575. doi: 10.1016/j.procs.2016.07.144.

Long Y, Xia GS, Li S, Yang W, Yang MY, Zhu XX, Li D. 2021. On creating benchmark dataset for aerial image interpretation: Reviews, guidances, and million-aid. IEEE Journal of selected topics in applied earth observations and remote sensing, 14, 4205–4230. doi: 10.1109/JSTARS.2021.3070368.

Lü ZY, Shi W, Zhang X, Benediktsson JA. 2018. Landslide inventory mapping from bitemporal high-resolution remote sensing images using change detection and multiscale segmentation. IEEE Journal of Selected Topics in Applied Earth Observations and Remote Sensing, 11(5), 1520–1532. doi: 10.1109/JSTARS.2018.2803784.

Meng J, Li CD, Zhou JQ, Zhang ZH, Yan SY, Zhang YH, Huang DW, Wang GH. 2023. Multiscale evolution mechanism of sandstone under wet-dry cycles of deionized water: from molecular scale to macroscopic scale. Journal of Rock Mechanics and Geotechnical Engineering, 15(5), 1171–85. doi: 10.1016/j.jrmge.2022.10.008.

Mohan A, Singh AK, Kumar B, Dwivedi R. 2021. Review on remote sensing methods for landslide detection using machine and deep learning. Transactions on Emerging Telecommunications Technologies, 32(7), e3998. doi: 10.1002/ett.3998.

Mondini AC, Guzzetti F, Reichenbach P, Rossi M, Cardinali M, Ardizzone F. 2011. Semi-automatic recognition and mapping of rainfall induced shallow landslides using optical satellite images. Remote sensing of environment, 115(7), 1743–1757. doi: 10.1016/j.rse.2011.03.006.

Qi T, Zhao Y, Meng X, Chen G, Dijkstra T. 2021. AI-Based susceptibility analysis of shallow landslides induced by heavy rainfall in Tianshui, China. Remote Sensing, 13(9), 1819. doi: 10.3390/rs13091819.

Ronneberger O, Fischer P, Brox T. 2015. U-Net: Convolutional networks for biomedical image segmentation. Medical Image Computing and Computer-Assisted Intervention (MICCAI), 9351, 234–241. doi: 10.48550/arXiv.1505.04597.

Sandler M, Howard A, Zhu M, Zhmoginov A, Chen LC. 2018. MobileNetV2: Inverted residuals and linear bottlenecks. In Proceedings of the IEEE conference on computer vision and pattern recognition, 4510–4520. doi: 10.48550/arXiv.1801.04381.

Simonyan K, Zisserman A. 2014. Very deep convolutional networks for large-scale image recognition. arXiv preprint arXiv: 1409.1556. doi: 10.48550/arXiv.1409.1556.

Solari L, Del SM, Raspini F, Barra A, Bianchini S, Confuorto P, Casagli

N, Crosetto M. 2020. Review of satellite interferometry for landslide detection in Italy. Remote Sensing, 12(8), 1351. doi: 10.3390/rs12081351.

Sun Q, Zhang L, Ding XL, Hu J, Li ZW, Zhu JJ. 2015. Slope deformation prior to Zhouqu, China landslide from InSAR time series analysis. Remote Sensing of Environment, 156, 45–57. doi: 10.1016/j.rse.2014.09.029.

Tieleman T, Hinton G. 2012. Lecture 6.5-RMSProp: Divide the gradient by a running average of its recent magnitude. COURSERA: Neural Networks for Machine Learning, 4, 26–31.

Wang H, Zhang L, Yin K, Luo H, Li J. 2021. Landslide identification using machine learning. Geoscience Frontiers, 12(1), 351–364. doi: 10.1016/j.gsf.2020.02.012.

Wei FQ, Sergey C, Konstantin A, Dmitry P, Olga T, Su PC, Jiang YH, Xu A, Alexey P. 2010. A seismically triggered landslide in the Niujuan Valley near the epicenter of the 2008 Wenchuan Earthquake. Journal of Earth Science, 21(6), 901–909. doi: 10.1007/s12583-010-0143-8.

Xu C, Li C, Cui Z, Zhang T, Yang J. 2020. Hierarchical semantic propagation for object detection in remote sensing imagery. IEEE Transactions on Geoscience and Remote Sensing, 58(6), 4353–4364. doi: 10.1109/TGRS.2019.2963243.

Zhang TL, Zhou AG, Sun Q, Wang HS, Wu JB, Liu ZH. 2020. Hydrological response characteristics of landslides under typhoon-triggered rainstorm conditions. China Geology, 3(3), 455–461. doi: 10.31035/cg2020028.

Zhang X, Yu W, Pun MO, Shi W. 2023. Cross-domain landslide mapping from large-scale remote sensing images using prototype-guided domain-aware progressive representation learning. ISPRS Journal of Photogrammetry and Remote Sensing, 197, 1–17. doi: 10.1016/j.isprsjprs.2023.01.018.

Zhao C, Lu Z. 2018. Remote Sensing of Landslides—A Review. Remote Sensing, 10(2), 279. doi: 10.3390/rs10020279.

Zhong C, Li H, Xiang W, Su AJ, Huang XF. 2012. Comprehensive study of landslides through the integration of multi remote sensing techniques: Framework and latest advances. Journal of Earth Science, 23(2), 243–252. doi: 10.1007/s12583-012-0245-6.

Zhou PC, Cheng G, Yao XW, Han JW. 2021. Machine learning paradigms in high-resolution remote sensing image interpretation. National Remote Sensing Bulletin, 25(1), 182–197. doi: 10.11834/jrs.20210164.

Zhu XX, Tuia D, Mou L, Xia GS, Zhang L, Xu F, Fraundorfer F. 2017. Deep learning in remote sensing: A comprehensive review and list of resources. IEEE Geoscience and Remote Sensing Magazine, 5(4), 8–36. doi: 10.1109/MGRS.2017.2762307.